magnetochemistry

MDPI

Article

Analysis of the Anisotropic Magnetocaloric Effect in RMn_2O_5 Single Crystals

Mohamed Balli [1,2,*], Saber Mansouri [2], Serge Jandl [1,2], Patrick Fournier [1,2,3] and Dimitre Z. Dimitrov [4,5]

1 Institut Quantique, Université de Sherbrooke, Sherbrooke, QC J1K 2R1, Canada; serge.jandl@usherbrooke.ca (S.J.); patrick.fournier@usherbrooke.ca (P.F.)
2 Regroupement québécois sur les matériaux de pointe, Département de physique, Université de Sherbrooke, Sherbrooke, QC J1K 2R1, Canada; Saber.Mansouri@USherbrooke.ca
3 Canadian Institute for Advanced Research, Toronto, Ontario M5G 1Z8, Canada
4 Institute of Solid State Physics, Bulgarian Academy of Science, Sofia 1184, Bulgaria; ddimitrov@iomt.bas.bg
5 Institute of Optical Materials and Technologies, Bulgarian Academy of Sciences, Sofia 1113, Bulgaria
* Correspondence: Mohamed.balli@usherbrooke.ca

Received: 6 October 2017; Accepted: 8 November 2017; Published: 21 November 2017

Abstract: Thanks to the strong magnetic anisotropy shown by the multiferroic RMn_2O_5 (R = magnetic rare earth) compounds, a large adiabatic temperature change can be induced (around 10 K) by rotating them in constant magnetic fields instead of the standard magnetization-demagnetization method. Particularly, the $TbMn_2O_5$ single crystal reveals a giant rotating magnetocaloric effect (RMCE) under relatively low constant magnetic fields reachable by permanent magnets. On the other hand, the nature of R^{3+} ions strongly affects their RMCEs. For example, the maximum rotating adiabatic temperature change exhibited by $TbMn_2O_5$ is more than five times larger than that presented by $HoMn_2O_5$ in a constant magnetic field of 2 T. In this paper, we mainly focus on the physics behind the RMCE shown by RMn_2O_5 multiferroics. We particularly demonstrate that the rare earth size could play a crucial role in determining the magnetic order, and accordingly, the rotating magnetocaloric properties of RMn_2O_5 compounds through the modulation of exchange interactions via lattice distortions. This is a scenario that seems to be supported by Raman scattering measurements.

Keywords: RMn_2O_5; multiferroics; anisotropy; single crystals; magnetocaloric effect; Raman scattering

1. Introduction

Functional magnetocaloric materials at room temperature have attracted worldwide interest over the last two decades due to their potential implementation as refrigerants in magnetic cooling systems [1–13]. However, the search for materials with excellent magnetocaloric properties in the temperature range from about 2 to 30 K is of great interest from fundamental, practical, and economical points of view, due to their potential use as refrigerants in several low temperature applications such as the space industry, scientific instruments, and gas liquefaction [14–25]. On the other hand, the development of new designs that can render magnetic cooling more competitive is also a key parameter for the commercialization of this emergent technology. Recently, Matsumoto et al. [14] have unveiled a reciprocating AMR magnetic cooling device which utilizes the $Dy_{2.4}Gd_{0.6}Al_5O_{12}$ (DGAG) compound as a working refrigerant. However, this material exhibits a large specific heat which largely reduces its magnetocaloric effect (MCE) in terms of the adiabatic temperature change (1 to 2 K under 1 T) [14].

In this context, the RMn_2O_5 (R = magnetic rare-earth element) multiferroics seem to be alternative candidates for magnetocaloric tasks around 10 K [15,16,25–29]. These compounds unveil complex crystalline and magnetic structures which results in a wide range of fascinating electrical and magnetic

phenomena [25–29]. At room temperature, they crystallize in the orthorhombic structure of the space group Pbam. Their unit cell consists of $Mn^{3+}O_5$ pyramids and $Mn^{4+}O_6$ octahedra which are connected to each other through oxygen atoms [25,26]. The octahedra are aligned along the *c*-axis and share their edges. The formed ribbons are linked by pairs of corner-shared $Mn^{3+}O_5$ pyramids within the ab-plane. The rare earth R^{3+} ions are located in the empty interstitial sites surrounded by octahedra and pyramids.

Over the past fifteen years, the RMn_2O_5 compounds have been widely studied because of the strong coupling between their electric and magnetic ordering parameters. Particularly, Hur et al. [13] have demonstrated that a reversible switching of electric polarization can be achieved in $TbMn_2O_5$ using relatively low magnetic fields, opening ways for the design of new multiferroic devices. On the other hand, the competition between different magnetic exchange interactions in the orthorhombic RMn_2O_5 compounds results in strongly frustrated systems. Consequently, a large MCE could be obtained by rotating them between their easy and hard-axes in constant magnetic fields (Figure 1), instead of the conventional magnetization-demagnetization process (via field variation) [15,16,30,31]. This would enable the implementation of more compact and efficient magnetic refrigeration devices with a simplified design [1,15,16]. However, as presented below, the RMCE shown by the RMn_2O_5 oxides markedly depends on the rare earth element. In this paper, we try to understand the physics behind such differences by combining both magnetic measurements and Raman scattering data.

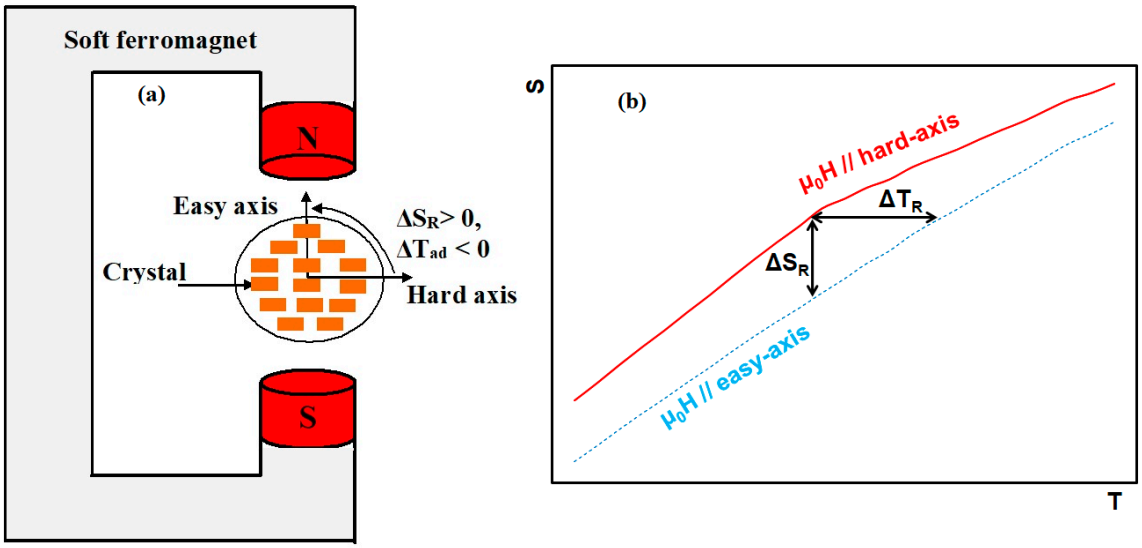

Figure 1. (**a**) Generation of the MCE by rotating the single crystals between their easy and hard-axes; (**b**) Full entropy as a function of temperature along the easy and hard-axes.

It is worth noting that the magnetocaloric properties and particularly the RMCE were separately reported in RMn_2O_5 (R = Ho, Tb) multiferroics [15,16]. However, in order to provide the reader with the big picture of the RMCE shown by these materials, we consider that it is important to firstly discuss and compare their magnetic and magnetocaloric properties in Section 2. This will enable us to pave the way for the developed analysis in Section 3 regarding the influence of the rare earth size on the RMCE in RMn_2O_5 single crystals.

2. RMCE in RMn_2O_5 (R = Tb and Ho): Comparative Study

Figure 2 shows the Raman spectra of RMn_2O_5 (R = Tb and Ho) at 5 K obtained with incident light (632.8 nm) polarized in the xy-plane. The analysis of different Raman excitations confirms that the high-quality crystals under study form in an orthorhombic symmetry with the Pbam space group. It is worth noting that the competition between different magnetic exchange interactions

makes RMn_2O_5 systems highly frustrated. Consequently, consecutive magnetic and ferroelectric phase transitions occur at around 45, 38, 20, and 10 K [25–29]. Usually, the Mn^{3+}/Mn^{4+} spins order in an incommensurate antiferromagnetic (AFM) state at T_{N1} ~45 K, becoming commensurate with decreasing temperature at a lock-in transition point (T_L = 33 K). A second magnetic phase transition at which the AFM ordering of Mn moments becomes incommensurate takes place at T_{N2} ~20 K. The onset of ferroelectric order was observed slightly below T_{N1}, at T_C ~38 K, while the rare earth moments usually order below 15 K [25–29]. The temperature dependence of the magnetization for both $HoMn_2O_5$ and $TbMn_2O_5$ compounds under a low magnetic field of 0.1 T applied along their easy-axes is reported in Figure 3a. As shown, only the magnetic transition related to the R^{3+} spin ordering is clearly visible at low temperatures around 10 K. The phase transitions involving the manganese sublattice and occurring at T_{N1}, T_C, and T_{N2} cannot be clearly seen in the thermomagnetic curves shown in Figure 3a, but their presence can be easily identified from specific heat measurements, as reported in Reference [28]. This mainly arises from the complex arrangement of the Mn moments in RMn_2O_5. In the latter, the Mn^{3+}/Mn^{4+} magnetic moments are strongly AFM-coupled within the ab-plane, building zigzag chains in a direction along the a-axis, regardless of the presence of the rare-earth 4f-magnetic moments [25,26]. This makes the contribution of the Mn^{3+}/Mn^{4+} moments to the total magnetization marginal, being a common property of RMn_2O_5 multiferroics [25–29]. On the other hand, the large magnetic moment of the rare earth ions (~10 μ_B) tends to overshadow the features resulting from the Mn sublattice.

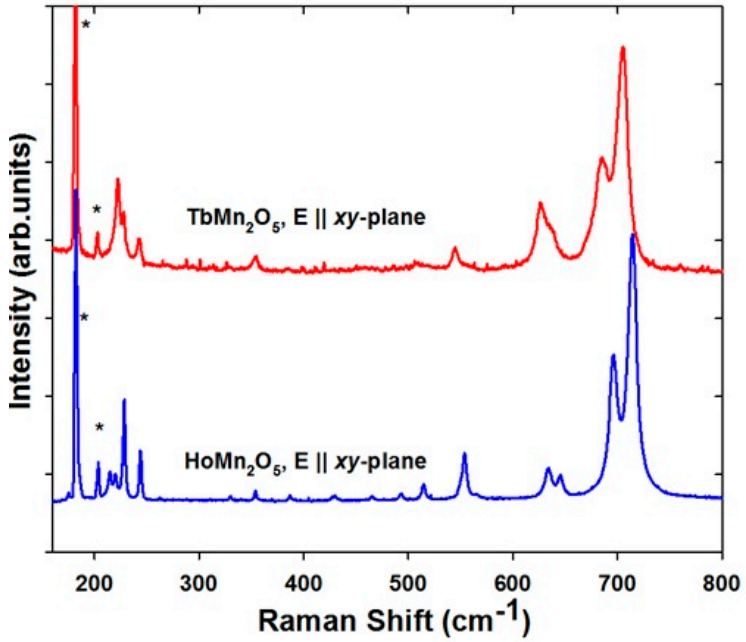

Figure 2. Micro Raman spectra at 5 K for the orthorhombic single crystals RMn_2O_5 (R = Ho, Tb). The narrow excitations demonstrate the high quality of the crystals and confirm the orthorhombic symmetry.

The magnetic and magnetocaloric properties (particularly RMCE) are very sensitive to the nature of the R^{3+} ions. In Figure 3b, the isothermal magnetization curves of the RMn_2O_5 (R = Ho, Tb) single crystals measured at 2 K as a function of the magnetic field applied along their easy and hard-axes are plotted. Although the magnetic moments of Tb^{3+} and Ho^{3+} are almost similar, the magnetic behaviors of both $TbMn_2O_5$ and $HoMn_2O_5$ show significant deviations. The data in Figure 3b indicate that the magnetic easy-direction of $TbMn_2O_5$ is along the *a*-axis, while that of $HoMn_2O_5$ is along the *b*-axis. From the linear fit of the inverse magnetic susceptibility (not shown here), the paramagnetic Curie-Weiss temperatures along the easy axes were found to be about 0.9 K for $HoMn_2O_5$ and 20 K for

$TbMn_2O_5$. The weak value of T_θ in the case of $HoMn_2O_5$ reflects a paramagnetic behavior and/or a weak antiferromagnetic order of Ho^{3+} ions. In contrast, the relatively large positive value of T_θ as in the case of $TbMn_2O_5$ suggests a dominant ferromagnetic ordering of Tb^{3+} moments. This leads to a marked difference in the behavior of the field dependence of magnetization along the easy-axes of RMn_2O_5 (R = Ho, Tb), as shown in Figure 3b. With an increasing field, the $HoMn_2O_5$ magnetization increases slightly with a weak tendency to saturate even under high magnetic fields (127 Am^2/kg under 7 T). For $TbMn_2O_5$, the magnetization easily reaches the saturation state under relatively low magnetic fields of about 2 T. The magnetization saturation is found to be about 140 Am^2/kg (8.75 μ_B/f.u.), being close to the Tb^{3+} magnetic moment (9 μ_B). This indicates that the Tb^{3+} magnetic moments in $TbMn_2O_5$ can be completely aligned using magnetic fields higher than 2 T, since the contribution of the Mn sublattice to the full magnetization is negligible.

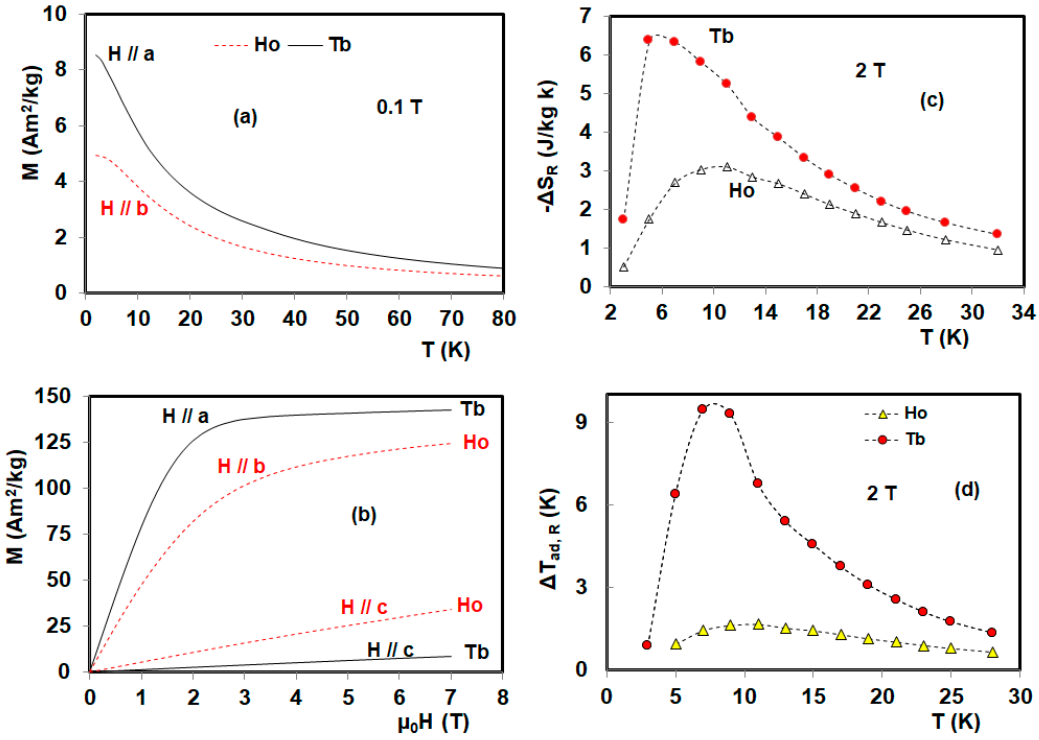

Figure 3. (**a**) Temperature dependence of magnetization under a magnetic field of 0.1 T applied along the easy-axes for $TbMn_2O_5$ and $HoMn_2O_5$. (**b**) Isothermal magnetization curves of RMn_2O_5 (R = Ho, Tb) measured at 2 K under magnetic fields applied along their easy and hard-axes. (**c**) Temperature dependence of the rotating isothermal entropy change in RMn_2O_5 (R = Ho, Tb) under 2 T. (**d**) Associated adiabatic temperature change under 2 T.

As a result, an enhancement of the magnetocrystalline anisotropy is observed in $TbMn_2O_5$ (Figure 3b). When changing the magnetic field direction from the easy-axis to the hard-axis, the magnetization under a magnetic field of 7 T is reduced by 94% in the case of $TbMn_2O_5$ and 70% for $HoMn_2O_5$. In Figure 3c, we report the temperature dependence of the rotating entropy change (ΔS_R), associated with the rotation by an angle of 90° of $HoMn_2O_5$ (in the cb-plane) and $TbMn_2O_5$ (in the ca-plane) between their easy and hard-axes. ΔS_R can be written as $\Delta S_R = \Delta S$ *(H//easy-axis)* $- \Delta S$ *(H//hard-axis)* [1], where ΔS *(H//easy-axis)* and ΔS *(H//hard-axis)* are the entropy changes resulting from the application of the magnetic field along the easy and hard-axes, respectively. Both quantities can be well calculated from isothermal magnetization curves using the Maxwell relation since the hysteresis effect in these multiferroic materials is negligible [32,33]. As can be seen in Figure 3c, $TbMn_2O_5$ unveils a rotating entropy change that is about two times larger than

that shown by $HoMn_2O_5$. Under a constant magnetic field of 2 T which is accessible via permanent magnets [34,35], $\Delta S_{R,\,max}$ is found to be 6.36 J/kg K for $TbMn_2O_5$ and only about 3 J/kg K for $HoMn_2O_5$. The improvement of ΔS_R in the $TbMn_2O_5$ compound is mainly attributed to the reinforcement of the magnetocrystalline anisotropy, as well as the enhancement of the magnetization (arising from Tb^{3+} ions) along the easy-axis. More interestingly, $TbMn_2O_5$ presents a rotating adiabatic temperature change ($\Delta T_{R,\,ad}$) that is about five times larger than that obtained with $HoMn_2O_5$ under 2 T (Figure 3d). For both $HoMn_2O_5$ and $TbMn_2O_5$, $\Delta T_{R,\,ad}$ was evaluated using the equation $\Delta T_{R,ad} = -\frac{T}{C_P(H=0)}\Delta S_R$ where C_p is the specific heat. C_p values were taken from Reference [28].

Considering initially the magnetic field parallel to the hard-axis, the rotation motion around the intermediate-axis by an angle of 90° induces a maximum temperature change larger than 8 K for $TbMn_2O_5$ and only 1.6 K for $HoMn_2O_5$ under a constant magnetic field of 2 T. The giant $\Delta T_{R,\,ad}$ shown by $TbMn_2O_5$ is particularly due to its low specific heat and large rotating isothermal change. Around the ordering point of the rare earth moments, $TbMn_2O_5$ has a specific heat of about 6.8 J/kg K, being three times lower than that exhibited by $HoMn_2O_5$ [28]. In fact, the more ordered Tb^{3+} moments would reduce the magnetic part, and accordingly, the total specific heat.

3. Distinguished Features of the RMCE in RMn_2O_5: Hypothesis

It is worth noting that the fundamental mechanisms behind the coupling between the magnetic ordering, crystal structure, and magnetocaloric properties in RMn_2O_5 are still unclear. However, according to available data [25,26], we first speculate that the R^{3+} spins ordering, magnetic anisotropy, and accordingly, the strength of the rotating magnetocaloric effect in RMn_2O_5 multiferroics could be strongly controlled by the atomic radius of the magnetic rare earth ions. This can be well understood when considering the interplay between lattice distortions and exchange interactions. Looking at the RMn_2O_5 crystallographic structure [25,26], the Mn^{3+} (S = 2) and Mn^{4+} (S = 3/2) spins are ordered within the ab-plane in loops of five Mn following the arrangement Mn^{4+}-Mn^{3+}-Mn^{3+}-Mn^{4+}-Mn^{3+}. Based on the crystalline structure, the magnetic exchange interactions are mainly driven by the five nearest-neighbors of the Mn lattice identified as Mn^{4+}-O2-Mn^{4+} (J_1), Mn^{4+}-O3-Mn^{4+} (J_2), Mn^{4+}-O4-Mn^{3+} (J_3), Mn^{4+}-O3-Mn^{3+} (J_4), and Mn^{3+}-O1-Mn^{3+} (J_5) [25,26]. According to the Goodenough-Kanamori-Anderson rules [36–38] and the Mn-O-Mn bond angles associated with the exchange interactions in RMn_2O_5 (R = Ho, Tb) [26], it seems that J_3 and J_4 reinforce the ferromagnetic interactions of Mn^{4+} magnetic moments located in adjacent edge-shared octahedra, either side of the R^{3+} layer (with interaction J_1) [25,26]. This could explain the marked difference in terms of magnetic and magnetocaloric behaviours between $TbMn_2O_5$ and $HoMn_2O_5$ compounds. In fact, the interaction between the nearest Mn^{4+} spins is strongly modulated by the radius of the rare earth. As reported by Blake et al. [26], the Mn^{4+}-O2-Mn^{4+} bond angle increases when increasing the R^{3+} size. At 60 K, it was found to increase from 97.10° in the case of R = Ho to 97.45° for Tb, consequently increasing the corresponding interatomic distance Mn^{4+}-Mn^{4+} from 2.887 to 2.902 Å. Hence, the resulting interactions may play a role in determining the magnetic arrangement of R^{3+} via the local magnetic field produced by Mn^{4+} ions, and accordingly, the rotating magnetocaloric effect in RMn_2O_5 compounds. This scenario seems to be supported by Raman scattering investigations. The temperature dependences of the ~630 cm^{-1} Ag mode of RMn_2O_5 (R = Tb and Ho) are reported in Figure 4. For both, the frequency of this phonon (Mn-O stretching mode) deviates from the regular anharmonic behavior and hardens below T* ~ 65 K. According to early studies [39–41], T* is a characteristic temperature attributed to the short magnetic correlations often observed just above the Néel transition temperature [39–41]. This frequency hardening is due to the reduction of the unit cell volume below T* and T_N previously observed in RMn_2O_5 (R = Tb, Ho and Bi) ($\Delta\omega \approx -\gamma\cdot\omega_0\cdot\Delta V/V$) [39–41]. This volume contraction was attributed to the Mn-Mn exchange-striction [39–41]. The frequency hardening of the 630 cm^{-1} mode in $TbMn_2O_5$ (~1 cm^{-1}) is two times larger than its equivalent in $HoMn_2O_5$ (~0.5 cm^{-1}). This result underlines the importance of the lattice effect (R^{3+} size) on the Mn exchange interactions and therefore

on the ordering of R^{3+} magnetic moments. However, the crystalline field effect on the 4f magnetic moments ground state manifold may also play a role in the magnetic configuration of the R^{3+} spins. This scenario is currently being explored by our group.

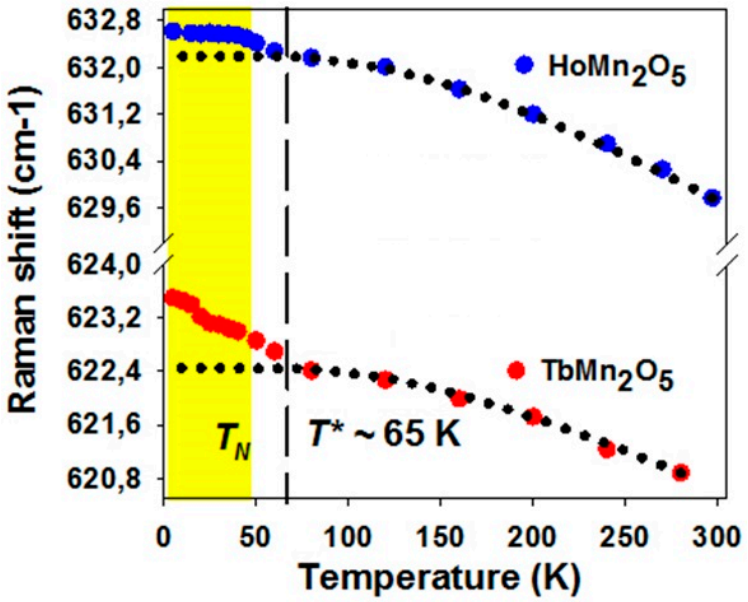

Figure 4. Temperature dependence of the Raman-active phonon ~630 cm^{-1} Ag for RMn_2O_5 (R = Ho, Tb).

4. Materials and Methods

The RMn_2O_5 (R = Ho, Tb) single crystals were synthesized by the high temperature solutions growth method using PbO-PbF_2-B_2O_3 flux, as described in Reference [29]. The RMn_2O_5 (R = Ho, Tb) polycrystalline samples were obtained first by mixing the R_2O_3 (R = Ho, Tb) and MnO_2 oxides in stoichiometric proportions using a standard solid-state reaction method. The resulting products were subjected to heat treatment in open air at 1150 °C for 48 h. Powders of RMn_2O_5 (R = Ho, Tb) were then mixed with PbO-PbF_2-B_2O_3 flux and pre-melted in a Pt crucible at 1225 °C for 48 h in oxygen atmosphere. The single crystal growth was achieved by reducing the growth temperature from 1225 °C to 1000 °C at a rate of 1 °C/h for $TbMn_2O_5$ and from 1225 °C to 950 °C at a rate of 0.5 °C/h for $HoMn_2O_5$ [29]. The crystals' crystallographic symmetry was analyzed based on Raman scattering. Micro-Raman spectra were collected using a Labram-800 equipped with a microscope, He-Ne laser, and a nitrogen-cooled charge coupled device detector (CCD). The magnetization measurements were carried out with a superconducting quantum interference devices (SQUID) magnetometer from Quantum Design (MPMS XL).

5. Conclusions

In summary, we have discussed the MCE features of RMn_2O_5 (R =Ho, Tb) single crystals with the support of both magnetization and Raman scattering data. This preliminary study particularly aims to clarify the origin of the marked difference between their RMCEs. According to Raman scattering data combined with magnetic measurements and early reported neutron diffraction experiments, it seems that the rare earth size could impact the RMn_2O_5 magnetocaloric properties. This could occur via the fine tuning of the magnetic exchange interactions involving the Mn sublattice because of structural distortions. The new established interactions would affect the ordering state of R^{3+} magnetic moments, and accordingly, the RMCE. However, this is not the only hypothesis to be considered since additional factors such as the crystalline field contribution must be taken into account. The latter is currently under investigation and any relevant result will be published in the future.

Additionally, to get the "big picture" of the RMn_2O_5 magnetocaloric features, this study must be completed by considering other rare earth elements such as Dy, Gd, Er, Pr ... etc. With the present work, we particularly aim at opening the door for further fundamental investigations of this promising family of multiferroics that can be implemented in numerous potential applications such as magnetic cooling and spintronic devices.

Acknowledgments: The authors thank M. Castonguay, S. Pelletier and B. Rivard for technical support. We acknowledge the financial support from NSERC (Canada), FQRNT (Québec), CFI, CIFAR, Canada First Research Excellence Fund (Canada), and the Université de Sherbrooke.

Author Contributions: M.B. conceived the work, performed magnetic measurements, prepared Figures and analyzed data, and wrote the paper; S.M. performed Raman scattering measurements and prepared figures; M.B., S.M., S.J., and P.F. discussed the results and revised the paper; D.Z.D. prepared the single crystals.

Conflicts of Interest: The authors declare no conflict of interest.

References

1. Balli, M.; Jandl, S.; Fournier, P.; Kedous-Lebouc, A. Advanced materials for magnetic cooling: Fundamentals and practical aspects. *Appl. Phys. Rev.* **2017**, *4*, 021305. [CrossRef]
2. Sari, O.; Balli, M. From conventional to magnetic refrigerator technology. *Int. J. Refrig.* **2014**, *37*, 8–15. [CrossRef]
3. Balli, M.; Sari, O.; Zamni, L.; Mahmed, C.; Forchelet, J. Implementation of La (Fe, Co)$_{13-x}$Si$_x$ materials in magnetic refrigerators: Practical aspects. *Mater. Sci. Eng. B* **2012**, *177*, 629–634. [CrossRef]
4. Moya, X.; Kar-Narayan, S.; Mathur, N.D. Caloric materials near ferroic phase transitions. *Nat. Mater.* **2014**, *13*, 439–450. [CrossRef] [PubMed]
5. Pecharsky, V.K.; Gschneidner, K.A., Jr. Giant Magnetocaloric Effect in $Gd_5Ge_2Si_2$. *Phys. Rev. Lett.* **1997**, *78*, 4494. [CrossRef]
6. Wada, H.; Tanabe, Y. Giant magnetocaloric effect of MnAs$_{1-x}$Sb$_x$. *Appl. Phys. Lett.* **2001**, *79*, 3302. [CrossRef]
7. Balli, M.; Fruchart, D.; Gignoux, D.; Dupuis, C.; Kedous-Lebouc, A.; Zach, R. Giant magnetocaloric effect in $Mn_{1-x}(Ti_{0.5}V_{0.5})_x$As: Experiments and calculations. *J. Appl. Phys.* **2008**, *103*, 103908. [CrossRef]
8. Balli, M.; Fruchart, D.; Gignoux, D.; Tobola, J.; Hlil, E.K.; Wolfers, P.; Zach, R. Magnetocaloric effect in ternary metal phosphides $(Fe_{1-x}Ni_x)_2$ P. *J. Magn. Magn. Mater.* **2007**, *316*, 358–360. [CrossRef]
9. Tegus, O.; Brück, E.; Buschow, K.H.J.; De Boer, F.R. Transition-metal-based magnetic refrigerants for room temperature applications. *Nature* **2002**, *415*, 150–152. [CrossRef] [PubMed]
10. Fujita, A.; Fujieda, S.; Hasegawa, Y.; Fukamichi, K. Itinerant-electron metamagnetic transition and large magnetocaloric effects in La$(Fe_xSi_{1-x})_{13}$ compounds and their hydrides. *Phys. Rev. B* **2003**, *67*, 104416. [CrossRef]
11. Hu, F.X.; Shen, B.G.; Sun, J.R.; Wang, G.J.; Cheng, Z.H. Very large magnetic entropy change near room temperature in $LaFe_{11.2}Co_{0.7}Si_{1.1}$. *Appl. Phys. Lett.* **2002**, *80*, 826–828. [CrossRef]
12. Balli, M.; Fruchart, D.; Gignoux, D. The $LaFe_{11.2}Co_{0.7}Si_{1.1}C_x$ carbides for magnetic refrigeration close to room temperature. *Appl. Phys. Lett.* **2008**, *92*, 232505. [CrossRef]
13. Balli, M.; Fruchart, D.; Gignoux, D. Optimization of La (Fe, Co)$_{13-x}$Si$_x$ based compounds for magnetic refrigeration. *J. Phys. Condens. Matter* **2007**, *19*, 236230. [CrossRef]
14. Matsumoto, K.; Kondo, T.; Yoshioka, S.; Kamiya, K.; Numazawa, T. Magnetic refrigerator for hydrogen liquefaction. *J. Phys. Conf. Ser.* **2009**, *150*, 012028. [CrossRef]
15. Balli, M.; Jandl, S.; Fournier, P.; Gospodinov, M.M. Anisotropy-enhanced giant reversible rotating magnetocaloric effect in $HoMn_2O_5$ single crystals. *Appl. Phys. Lett.* **2014**, *104*, 232402. [CrossRef]
16. Balli, M.; Jandl, S.; Fournier, P.; Dimitrov, D.Z. Giant rotating magnetocaloric effect at low magnetic fields in multiferroic $TbMn_2O_5$ single crystals. *Appl. Phys. Lett.* **2016**, *108*, 102401. [CrossRef]
17. Jin, J.L.; Zhang, X.Q.; Li, G.K.; Cheng, Z.H.; Zheng, L.; Lu, Y. Giant anisotropy of magnetocaloric effect in $TbMnO_3$ single crystals. *Phys. Rev. B* **2011**, *83*, 184431. [CrossRef]
18. Balli, M.; Jandl, S.; Fournier, P.; Mansouri, S.; Mukhin, A.; Ivanov, Y.V.; Balbashov, A.M. On the magnetocaloric effect in the multiferroic hexagonal $DyMnO_3$ single crystals. *J. Magn. Magn. Mater.* **2015**, *374*, 252–257. [CrossRef]

19. Jin, J.L.; Zhang, X.Q.; Ge, H.; Cheng, Z.H. Rotating field entropy change in hexagonal $TmMnO_3$ single crystal with anisotropic paramagnetic response. *Phys. Rev. B* **2012**, *85*, 214426. [CrossRef]
20. Balli, M.; Mansouri, S.; Jandl, S.; Fournier, P.; Dimitrov, D.Z. Large rotating magnetocaloric effect in the orthorhombic $DyMnO_3$ single crystal. *Solid State Commun.* **2016**, *239*, 9–13. [CrossRef]
21. Li, L.; Namiki, T.; Huo, D.; Qian, Z.; Nishimura, K. Two successive magnetic transitions induced large refrigerant capacity in HoPdIn compound. *Appl. Phys. Lett.* **2013**, *103*, 222405. [CrossRef]
22. Midya, A.; Das, S.N.; Mandal, P.; Pandya, S.; Ganesan, V. Anisotropic magnetic properties and giant magnetocaloric effect in antiferromagnetic $RMnO_3$ crystals (R = Dy, Tb, Ho, and Yb). *Phys. Rev. B* **2011**, *84*, 235127. [CrossRef]
23. Balli, M.; Roberge, B.; Vermette, J.; Jandl, S.; Fournier, P.; Gospodinov, M.M. Magnetocaloric properties of the hexagonal $HoMnO_3$ single crystal revisited. *Phys. B* **2015**, *478*, 77–83. [CrossRef]
24. Balli, M.; Roberge, B.; Jandl, S.; Fournier, P.; Palstra, T.T.M.; Nugroho, A.A. Observation of large refrigerant capacity in the $HoVO_3$ vanadate single crystal. *J. Appl. Phys.* **2015**, *118*, 073903. [CrossRef]
25. Noda, Y.; Kimura, H.; Fukunaga, M.; Kobayashi, S.; Kagomiya, I.; Kohn, K. Magnetic and ferroelectric properties of multiferroic RMn_2O_5. *J. Phys. Condens. Matter* **2008**, *20*, 434206. [CrossRef]
26. Blake, G.R.; Chapon, L.C.; Radaelli, P.G.; Park, S.; Hur, N.; Cheong, S.W.; Rodriguez-Carvajal, J. Spin structure and magnetic frustration in multiferroic RMn_2O_5 (R = Tb, Ho, Dy). *Phys. Rev. B* **2005**, *71*, 214402. [CrossRef]
27. Hur, N.; Park, S.; Sharma, P.A.; Ahn, J.S.; Guha, S.; Cheong, S.W. Electric polarization reversal and memory in a multiferroic material induced by magnetic fields. *Nature* **2004**, *429*, 392–395. [CrossRef] [PubMed]
28. Hur, N.; Park, S.; Sharma, P.A.; Guha, S.; Cheong, S.W. Colossal Magnetodielectric Effects in $DyMn_2O_5$. *Phys. Rev. Lett.* **2004**, *93*, 107207. [CrossRef] [PubMed]
29. Mihailova, B.; Gospodinov, M.M.; Güttler, B.; Yen, F.; Litvinchuk, A.P.; Iliev, M.N. Temperature-dependent Raman spectra of $HoMn_2O_5$ and $TbMn_2O_5$. *Phys. Rev. B* **2005**, *71*, 172301. [CrossRef]
30. Nikitin, S.A.; Skokov, K.P.; Koshkid'ko, Y.S.; Pastushenkov, Y.G.; Ivanova, T.I. Giant rotating magnetocaloric effect in the region of spin-reorientation transition in the $NdCo_5$ single crystal. *Phys. Rev. Lett.* **2010**, *105*, 137205. [CrossRef] [PubMed]
31. Kuz'min, M.D.; Tishin, A.M. Magnetic refrigerants for the 4.2-20 K region: Garnets or perovskites? *J. Phys. D Appl. Phys.* **1991**, *24*, 2039. [CrossRef]
32. Balli, M.; Fruchart, D.; Gignoux, D.; Zach, R. The "colossal" magnetocaloric effect in $Mn_{1-x}Fe_xAs$: What are we really measuring? *Appl. Phys. Lett.* **2009**, *95*, 072509. [CrossRef]
33. Balli, M.; Sari, O.; Fruchart, D.; Forchelet, J. Influence of the materials magnetic state on the accurate determination of the magnetocaloric effect. *Eur. Phys. J. Web Conf.* **2012**, *29*, 00005. [CrossRef]
34. Balli, M.; Sari, O.; Mahmed, C.; Besson, C.; Bonhote, P.; Duc, D.; Forchelet, J. A pre-industrial magnetic cooling system for room temperature application. *Appl. Energy* **2012**, *98*, 556–561. [CrossRef]
35. Sari, O.; Balli, M.; Trottet, G.; Bonhote, P.; Egolf, P.W.; Muller, C.; Heitzler, J.C.; Bour, S. Initial results of a test-bed magnetic refrigeration machine with practical running conditions. In Proceedings of the 3rd International Conference on Magnetic Refrigeration at Room Temperature, Des Moines, IA, USA, 11–15 May 2009; pp. 371–380.
36. Goodenough, J.B. Theory of the Role of Covalence in the Perovskite-Type Manganites [La, M(II)]MnO_3. *Phys. Rev.* **1955**, *100*, 564. [CrossRef]
37. Kanamori, J. Superexchange interaction and symmetry properties of electron orbitals. *J. Phys. Chem. Solids* **1959**, *10*, 87–98. [CrossRef]
38. Anderson, P.W. Theory of magnetic exchange interactions: Exchange in insulators and semiconductors. *Solid State Phys.* **1963**, *14*, 99–214.
39. Garcia-Flores, A.F.; Granado, E.; Martinho, H.; Urbano, R.R.; Rettori, C.; Golovenchits, E.I.; Sanina, V.A.; Oseroff, S.B.; Park, S.; Cheong, S.-W. Anomalous phonon shifts in the paramagnetic phase of multiferroic RMn_2O_5 (R = Bi, Eu, Dy): Possible manifestations of unconventional magnetic correlations. *Phys. Rev. B* **2006**, *73*, 104411. [CrossRef]

40. Chapon, L.C.; Blake, G.R.; Gutmann, M.J.; Park, S.; Hur, N.; Radaelli, P.G.; Cheong, S.W. Structural Anomalies and Multiferroic Behavior in Magnetically Frustrated $TbMn_2O_5$. *Phys. Rev. Lett.* **2004**, *93*, 177402. [CrossRef] [PubMed]
41. Granado, E.; Eleotério, M.S.; García-Flores, A.F.; Souza, J.A.; Golovenchits, E.I.; Sanina, V.A. Magnetoelastic and thermal effects in the $BiMn_2O_5$ lattice: A high-resolution x-ray diffraction study. *Phys. Rev. B* **2008**, *77*, 134101. [CrossRef]